REPORT NO. FRA-OR&D 75-53

DEVELOPMENT OF ANALYTICAL FIRE MODELS

L. Schalit
G. Schneyer
J. Toor
D. Laird

OCTOBER 1974
QUARTERLY PROGRESS REPORT

Prepared For
DEPARTMENT OF TRANSPORTATION
FEDERAL RAILROAD ADMINISTRATION
Office of Research and Development
Washington, D.C. 20590

NOTICE

Technical Report Documentation Page

1. Report No.	2. Government Accession No.	3. Recipient's Catalog No.
FRA-OR&D 75-53		

4. Title and Subtitle	5. Report Date
DEVELOPMENT OF ANALYTIC FIRE MODELS	October 1974
	6. Performing Organization Code
7. Author(s)	8. Performing Organization Report No.
L. Schalit, G. Schneyer, J. Toor, D. Laird	SSS-R-74-2436
9. Performing Organization Name and Address Systems, Science, and Software * Box 1620 La Jolla, California 92037	10. Work Unit No. (TRAIS)
	11. Contract or Grant No.
12. Sponsoring Agency Name and Address U.S. Department of Transportation Federal Railroad Administration Office of Research and Development Washington, D.C. 20590	13. Type of Report and Period Covered Progress Report (Jun 17, 1974 - Sept 16, 1974)
	14. Sponsoring Agency Code

15. Supplementary Notes

* Under contract to: National Aeronautics and Space Administration
Ames Research Center
Moffett Field, California 94035

16. Abstract

This report descirbes the progress from June 17, 1974 to September 16, 1974, in a project to develop analytic models of pool fires and torch fires.

17. Key Words	18. Distribution Statement
Fire Research, Fluid Mechanics, Turbulence	Document is available to the public through the National Technical Information Service, Springfield, Virginia 22161

19. Security Classif. (of this report)	20. Security Classif. (of this page)	21. No. of Pages	22. Price
Unclassified	Unclassified	66	

Form DOT F 1700.7 (8-72) Reproduction of completed page authorized

TABLE OF CONTENTS

SUMMARY

The hydrodynamic equations which include a turbulence model based on the work by Spalding's group have been derived along with the associated boundary and initial conditions. They have also been put into finite difference form, coded, and are currently being debugged. The soot chemical model has been determined and is included in the above formulation. A radiation code based on the long characteristics method has been prepared for inclusion into the code as a subroutine as has an equation of state package.

I. INTRODUCTION

The development of computer codes for the accurate characterization of torch and pool fires is a complex, multi-disciplinary task. In particular, the sciences and/or technologies of fluid mechanics, numerical analysis, chemistry, thermodynamics and radiation transport must be meshed together in order to produce codes capable of such an accurate characterization.

During the initial quarter of this contract, the emphasis has been on development of the components in the several aforementioned areas which can then be meshed together in succeeding quarters to form the torch and pool fire computer codes. Consequently, this initial quarterly progress report has been divided along technological lines. Thus, the next section reports on hydrodynamics and its associated elements, Section III discusses the equation of state package that has been developed, Section IV reports on the soot chemical model, and Section V discusses the radiation transport model and computer code. Finally, Section VI discusses the thrust of the effort in the next quarter.

II. HYDRODYNAMICS

The hydrodynamic model that S^3 is putting into the torch and pool fire codes is misleadingly similar to that found in the previous AROKEM[1] code. While the mean flow equations are only modestly modified, the addition of equations for the turbulence quantities complicates the system tremendously in that those equations apparently have never previously been derived for an axisymmetric flow with spatial density variations. Since the strength and accuracy of the characterization of the fires depends very heavily on this formulation, such complications must be accepted.

A goodly portion of this reporting period (admittedly somewhat more than had been originally planned) was spent deriving the proper set of differential equations. The details of the derivations will not be included in this report but will be issued later as a topical report. This topical report will include all of the details of the derivation of the controlling differential equations and associated boundary conditions for both the torch and pool fire codes, their transformation into a normalized stream function coordinate system, and their final conversion into difference equations. Here we will only quote some of the results and indicate the paths taken in the derivation.

2.1 THE CONSERVATION EQUATIONS IN THE r-x COORDINATE SYSTEM

The basic assumptions made in the derivation of the governing equations are that:

1. All mean quantities are steady (i.e., $\partial/\partial t = 0$).
2. The standard turbulent assumption involving the breakup of dynamic quantities into mean and fluctuating components is valid where the mean quantities are averaged over a time span long with respect to the time scale of the turbulent fluctuations but short with respect to the time scale of interest in the problem.
3. The turbulent fluctuations in mass density are negligible except insofar as they affect the buoyancy terms (only applicable to the pool fire).
4. Spalding-type modeling of certain turbulent fluctuation correlations in terms of mean quantities is valid.

With the above assumptions, the conservation equations in an r-x axisymmetric cylindrical coordinate system can be written.

2.1.1 Conservation of Mean Total Mass

$$\frac{\partial(\rho u r)}{\partial x} + \frac{\partial(\rho v r)}{\partial r} = 0 \qquad (2.1)$$

where ρ = total mass density (mass/vol)

u,v = mean axial and radial components of velocity (length/time)

x,r = axial and radial coordinate (length)

2.1.2 Conservation of Mean Axial Momentum

$$\frac{\partial(\rho u^2 r)}{\partial x} + \frac{\partial(\rho uvr)}{\partial r} + \frac{\partial(rP)}{\partial x} = \frac{\partial}{\partial r}\left[\left(\mu_\ell + \frac{C_\mu \rho k^2}{\varepsilon}\right) r \frac{\partial u}{\partial r}\right] - \frac{2}{3}\frac{\partial(\rho k r)}{\partial x} \qquad (2.2)$$

where

P = static pressure (force/area)

μ_ℓ = laminar dynamic viscosity coefficient (mass/length-time)

k = mean turbulent kinetic energy = $(\overline{\vec{u}' \cdot \vec{u}'})/2$ (energy/mass)

ε = mean turbulent dissipation rate = $\mu_\ell/\rho \; (\overline{\nabla \vec{u}' \cdot \text{def } \vec{u}'})$ (energy/mass-time)

$\mu_t \equiv C_\mu \rho k^2/\varepsilon$ = turbulent dynamic viscosity coefficient (mass/length-time)

$C_\mu = C_\mu(Re_t)$ Spalding coefficient of turbulent viscosity

Re_t = turbulent Reynolds' number = $\rho k^2/\varepsilon\mu_\ell$

Conservation of radial momentum in a boundary layer (a free jet is also a boundary layer) usually only contributes the information that $\partial P/\partial r = 0$, but here we find that the conservation of mean radial momentum in our boundary layer tells us that

$$\frac{\partial P}{\partial r} = -\frac{2}{3}\frac{\partial(\rho k)}{\partial r} \quad \text{or} \qquad (2.3a)$$

$$P + \frac{2}{3}\rho k = \Pi(x) \qquad (2.3b)$$

We can, therefore, substitute Eq. (2.3a) back into Eq. (2.2) to get the form of the mean axial conservation equation that we will use:

$$\frac{\partial(\rho u^2 r)}{\partial x} + \frac{\partial(\rho uvr)}{\partial r} + \frac{d(r\Pi)}{dx} = \frac{\partial}{\partial r}\left[\left(\mu_\ell + \frac{C_\mu \rho k^2}{\varepsilon}\right) r \frac{\partial u}{\partial r}\right] \qquad (2.2a)$$

In all of the succeeding equations, (2.3) has been substituted wherever applicable.

2.1.3 Conservation of Mean Species Mass

There are five species which we shall denote by 1 = fuel, 2 = oxygen, 3 = products, 4 = diluent, 5 = carbon soot. The conservation equations for 1 and 2 can be combined to yield

$$\frac{\partial(\rho u f_{12} r)}{\partial x} + \frac{\partial(\rho v f_{12} r)}{\partial r} = \frac{\partial}{\partial r}\left[\rho\left(D_2^\ell + \frac{C_\mu k^2}{\varepsilon \sigma_f}\right) r \frac{\partial f_{12}}{\partial r} + \rho(D_1^\ell - D_2^\ell)\, r \frac{\partial F_1}{\partial r}\right] \qquad (2.4)$$

where

F_j = mean mass fraction of species j

$f_{12} \equiv F_1 - F_2/a$

a = mass of oxygen combining stoichiometrically with unit mass of fuel

D_j^ℓ = laminar diffusion constant for species j (length^2/time)

σ_f = turbulent Schmidt number

The diluent conservation equation becomes:

$$\frac{\partial(\rho u F_4 r)}{\partial x} + \frac{\partial(\rho v F_4 r)}{\partial r} = \frac{\partial}{\partial r}\left[\rho\left(D_4^\ell + \frac{C_\mu k^2}{\varepsilon \sigma_f}\right) r \frac{\partial F_4}{\partial r}\right] \qquad (2.5)$$

Furthermore, since F_5 is always very small, we can say that

$$\sum_{j=1}^{4} F_j \tilde{=} 1 \qquad (2.6)$$

The conservation equation for soot is taken to be:

$$\frac{\partial(\rho u F_5 r)}{\partial x} + \frac{\partial(\rho v F_5 r)}{\partial r} = \frac{\partial}{\partial r}\left[\rho\left(D_5^{\ell} + \frac{C_\mu k^2}{\varepsilon \sigma_f}\right) r \frac{\partial F_5}{\partial r}\right] + r\left(\frac{dF_5}{dt}\right)_{chem} \qquad (2.6)$$

where the last term is the rate of soot production via chemical reaction and is discussed in Section IV.

Before proceeding to indicate how F_1, F_2, and F_3 can be deduced from f_{12} and f_4, we must calculate the RMS value of the turbulent fluctuations in f_{12}.

2.1.4 Conservation of Mean Square Species Fluctuations

$$\frac{\partial(\rho u G_{12} r)}{\partial x} + \frac{\partial(\rho v G_{12} r)}{\partial r} = C_G \frac{\rho k^2 r}{\varepsilon}\left(\frac{\partial f_{12}}{\partial r}\right)^2 + \frac{\partial}{\partial r}\left[\rho\left(D_2^{\ell} + \frac{C_\mu k^2}{\varepsilon \sigma_f}\right) r \frac{\partial G_{12}}{\partial r}\right] - C_f \frac{\varepsilon r G_{12}}{k} \qquad (2.7)$$

where

$G_{12} = \overline{(f'_{12})^2}$ = mean square of turbulent fluctuations in f_{12}

C_G, C_f = Spalding constants

We can now proceed to deduce F_1, F_2, and F_3. Let us define the "instantaneous" value of f_{12} over the first half of the averaging time scale to be constant and given by

$$f_{12}^{(1)} = f_{12} + G_{12}^{1/2} \tag{2.8a}$$

while over the second half it is constant and given by

$$f_{12}^{(2)} = f_{12} - G_{12}^{1/2} \tag{2.8b}$$

Now the basic assumption in all diffusion flames is that the chemical reaction rate is infinite so we must have, on an instantaneous basis, either only fuel and products or only oxygen and products present. Thus, we conclude that if

$$f_{12}^{(j)} \begin{cases} > 0, & F_1^{(j)} = f_{12}^{(j)},\ F_2^{(j)} = 0 \\ = 0, \text{ then} & F_1^{(j)} = F_2^{(j)} = 0 \\ < 0, & F_1^{(j)} = 0,\ F_2^{(j)} = -af_{12}^{(j)} \end{cases} \tag{2.9}$$

Since the mean is simply the average over the time scale, we have that

$$F_i = \frac{1}{2} \sum_{j=1}^{2} F_i^{(j)} \quad \text{for } i = 1,2 \tag{2.10}$$

It may be noted that the above technique is primarily aimed at reproducing the "unmixedness" phenomenon seen in turbulent diffusion flames but almost impossible to reproduce using traditional turbulence models.

With F_1, F_2, and F_4 now determined, a simple rearrangement of Eq. (2.6) yields

$$F_3 = 1 - (F_1 + F_2 + F_4) \tag{2.11}$$

2.1.5 Conservation of Mean Turbulent Kinetic Energy

If we take the scaler product of the turbulent velocity fluctuation, $\vec{u}'$, and the momentum equation, time average the result, and "Spalding-model" some of the terms, we get

$$\frac{\partial(\rho ukr)}{\partial x} + \frac{\partial(\rho vkr)}{\partial r} - \frac{2}{5\rho}\left[\frac{\partial(\rho^2 ukr)}{\partial x} + \frac{\partial(\rho^2 vkr)}{\partial r}\right]$$

$$= \frac{\partial}{\partial r}\left[r\left\{\left(\mu_\ell + \frac{3\mu_t}{5\sigma_k}\right)\frac{\partial k}{\partial r} + \frac{2\nu_\ell}{5}\, k\, \frac{\partial \rho}{\partial r}\right\}\right]$$

$$- \frac{2\nu_t r}{5\sigma_p}\frac{\partial(\rho k)}{\partial r}\frac{\partial \ln\rho}{\partial r} + \frac{3\mu_t r}{5}\left(\frac{\partial u}{\partial r}\right)^2 - \frac{3\rho\varepsilon r}{5} \qquad (2.12)$$

2.1.6 Conservation of Mean Turbulent Energy Dissipation Rate

This equation, for ε, was the most difficult to derive. It has supplanted the equation for turbulent vorticity (W) in the formulation originally presented in the proposal,[2] because recent information[3,4] has indicated that the k-ε model is somewhat superior to the k-W model and S³ believes that the complexity of the torch/pool fire problem and its practical importance warrants using the best model available. The difficulty in deriving the equation is possibly most easily appreciated when one realizes that it requires taking the vector gradient of the momentum equation and then taking the scaler product of the resulting tensorial equation with the tensor, def $\vec{u}'$ (the symmetric tensor which is the sum of the vector gradient of the turbulent fluctuation in velocity ($\nabla\vec{u}'$) and its transpose). While the derivation is difficult in Cartesian coordinates, its difficulty is compounded many-fold in cylindrical coordinates by the necessity of utilizing the somewhat esoteric mathematics of covariant/contravariant tensor analysis. The final result can be written as

$$\frac{\partial(\rho u \epsilon r)}{\partial x} + \frac{\partial(\rho v \epsilon r)}{\partial r} = \rho \frac{\partial}{\partial r}\left[r\left(\nu_\ell + \frac{C_\mu k^2}{\epsilon \sigma_\epsilon}\right)\frac{\partial \epsilon}{\partial r}\right] - \left[\frac{\nu_\ell r}{3}\frac{\partial \rho}{\partial r}\right]\frac{\partial \epsilon}{\partial r} - \left(\frac{C_2 r \rho}{k}\right)\epsilon^2 - \left[\frac{1}{3}\left(\frac{\partial(ru)}{\partial x} + \frac{\partial(rv)}{\partial r}\right) - \frac{C_1 C_\mu k r}{\epsilon}\left(\frac{\partial u}{\partial r}\right)^2\right]\rho\epsilon \qquad (2.13)$$

where

C_1 = Spalding constant

$C_2 = C_2(Re_t)$ = Spalding coefficient

2.1.7 Conservation of Mean Energy

$$\frac{\partial(\rho u h r)}{\partial x} + \frac{\partial(\rho v h r)}{\partial r} = \frac{\partial}{\partial r}\left[\left(\lambda_\ell + \frac{C_\mu \rho k^2}{\epsilon \sigma_h}\right) r \frac{\partial h}{\partial r}\right] + \frac{\partial}{\partial x}\left[ru\left(\Pi - \frac{2}{3}\rho k\right)\right] - \frac{2}{3}(rv\rho k) - \Pi\frac{\partial(ru)}{\partial x} + \frac{2}{3}\rho k\left[\frac{\partial(ru)}{\partial x} + \frac{\partial(rv)}{\partial r}\right] + \frac{2}{3\rho}\frac{\partial}{\partial r}\left[\frac{C_\mu \rho k^2}{\sigma_{p\epsilon}} r \frac{\partial(\rho k)}{\partial r}\right] + \rho\epsilon r + \mu_\ell r\left(\frac{\partial u}{\partial r}\right)^2 + rS_r \qquad (2.14)$$

where

λ_ℓ = laminar thermal diffusivity (length^2/time)

σ_h = turbulent Prandtl number

S_r = net radiation heat input (energy/time-volume)

h = total static specific enthalpy (energy/mass)

2.1.8 Equation of State

If we assume that h does not vary violently, we can use the equation of state to approximate equilibrium chemistry by defining

$$T^{(\alpha)} = T\left(F_j^{(\alpha)}, h\right) \qquad \alpha = 1,2 \tag{2.15a}$$

$$\left(\frac{P}{\rho}\right)^{(\alpha)} = P\left(F_j^{(\alpha)}, h\right) \tag{2.15b}$$

Then

$$T = \frac{1}{2}\left(T^{(1)} + T^{(2)}\right) \tag{2.16a}$$

$$\frac{P}{\rho} \equiv P = \frac{1}{2}\left(\frac{P}{\rho}\right)^{(1)} + \left(\frac{P}{\rho}\right)^{(2)} \tag{2.16b}$$

Combining Eq. (2.16b) with (2.3a) gives

$$\rho = \frac{\Pi(x)}{P + \frac{2}{3}k} \tag{2.17a}$$

$$P = \rho P \tag{2.17b}$$

which are determinate since $\Pi(x)$ is known from free-stream conditions and k from Eq. (2.12).

2.1.9 Initial Conditions

The terminology "initial conditions" is usually used in regard to temporally-dependent quantities with "boundary conditions" being used to denote spatially-dependent quantities. Because a jet moves in such a way that the streamwise coordinate is "time"-like, we will refer to the conditions at $x = x_0$, the jet origin, as being the initial conditions (I.C.'s) and use "boundary conditions" (B.C.'s) to denote only the conditions at the extremes (centerline and free-stream) of the cross-stream coordinate.

The I.C.'s for all of the quantities formally assume the same form, i.e.,

$$\phi(r,x_0) = \phi_0(r) \quad \text{for } 0 \leq r \leq R_0 \tag{2.18}$$

where ϕ, ϕ_0 represents any of the fourteen variables and R_0 = radius of jet at $x = x_0$ (length).

2.1.10 Boundary Conditions

The B.C.'s for the jet are nearly all identical but of mixed type. That is to say that at the centerline ($r = 0$), we have

$$\frac{\partial \phi}{\partial r}(0,x) = 0 \quad \text{for} \quad x \geq x_0 \tag{2.19}$$

where ϕ represents all of the variables except for v which can be shown to be

$$v(0,x) = 0 \quad \text{for} \quad x \geq x_0 \tag{2.20}$$

At the edge of the jet, we have

$$\phi(r_\infty, x) = \phi_\infty(x)$$
$$x \geq x_0 \qquad (2.21a)$$
$$v(r_\infty, x) = 0$$

since a cross-wind is not permitted. Again ϕ denotes all variables except v and r_∞ is the lateral extent of the jet.

2.2 THE CONSERVATION EQUATIONS IN THE ω-z COORDINATE SYSTEM

It is convenient to convert our equations from an r-x coordinate system to an ω-z coordinate system where

$$\omega = \frac{\psi(r,x)}{\psi_\infty(x)} \quad , \quad z = x \tag{2.22}$$

The stream function, ψ, is defined in the traditional manner as

$$\frac{\partial \psi}{\partial r} = \rho u r, \quad \frac{\partial \psi}{\partial x} = -\rho v r \tag{2.23}$$

so that

$$\psi(r,x) = \int_0^r \rho u r dr \quad \text{if} \quad \psi(0,x) = 0 \tag{2.24}$$

and

$$\psi_\infty(x) = \int_0^{r_\infty(x)} \rho u r dr \tag{2.25}$$

This transformation achieves two things; it eliminates v from the equations (albeit introducing ψ_∞), and it permits the jet to be zoned in a consistent manner over its entire length.

2.2.1 The Differential Equations

Conservation of Mean Axial Momentum

$$\frac{\partial u}{\partial z} = \left[\omega\left(\frac{d\ln\psi_\infty}{dz}\right)\right]\frac{\partial u}{\partial \omega} + \frac{\partial}{\partial \omega}\left[\left(\mu_\ell + \frac{C_\mu \rho k^2}{\varepsilon}\right)\frac{\rho u r^2}{\psi_\infty^2}\frac{\partial u}{\partial \omega}\right] - \frac{1}{\rho u}\frac{d\Pi}{dz} \tag{2.26}$$

Conservation of Mean Turbulent Kinetic Energy

$$\frac{\partial k}{\partial z} = \left[\omega\left(\frac{d\ln\psi_\infty}{dz}\right)\right]\frac{\partial k}{\partial \omega} + \frac{\partial}{\partial \omega}\left[\left(\mu_\ell + \frac{C_\mu \rho k^2}{\varepsilon \sigma_\varepsilon}\right)\frac{\rho u r^2}{\psi_\infty^2}\frac{\partial k}{\partial \omega}\right]$$
$$+ \frac{2}{3}\frac{\partial}{\partial \omega}\left[\frac{\mu_\ell u r^2}{\psi_\infty^2}\frac{\partial(\rho k)}{\partial \omega}\right] - \frac{2}{3}\left[\frac{C_\mu k^2 r^2 u}{\varepsilon \sigma_p \psi_\infty^2}\frac{\partial \rho}{\partial \omega}\right]\frac{\partial(\rho k)}{\partial \omega}$$
$$+ \frac{2}{3}\left[\frac{\partial \ln\rho}{\partial z} - \omega\left(\frac{d\ln\psi_\infty}{dz}\right)\frac{\partial \ln\rho}{\partial \omega}\right] k$$
$$+ \left[\frac{C_\mu \rho^2 u r^2}{\varepsilon \psi_\infty^2}\left(\frac{\partial u}{\partial \omega}\right)^2\right] k^2 - \left(\frac{\varepsilon}{u}\right) \tag{2.27}$$

Conservation of Mean Turbulent Energy Dissipation Rate

$$\frac{\partial \varepsilon}{\partial z} = \left[\omega\left(\frac{d\ln\psi_\infty}{dz}\right)\right]\frac{\partial \varepsilon}{\partial \omega} + \rho\frac{\partial}{\partial \omega}\left[\left(\mu_\ell + \frac{C_\mu \rho k^2}{\varepsilon \sigma_\varepsilon}\right)\frac{u r^2}{\psi_\infty^2}\frac{\partial \varepsilon}{\partial \omega}\right] - \left[\frac{\mu_\ell u r^2}{3\psi_\infty^2}\frac{\partial \rho}{\partial \omega}\right]\frac{\partial \varepsilon}{\partial \omega}$$
$$+ \frac{1}{3}\left[\frac{\partial \ln\rho}{\partial z} - \omega\left(\frac{d\ln\psi_\infty}{dz}\right)\frac{\partial \ln\rho}{\partial \omega}\right]\varepsilon - \left(\frac{C_2}{uk}\right)\varepsilon^2 + \left[\frac{C_1 C_\mu \rho^2 k u r^2}{\psi_\infty^2}\left(\frac{\partial u}{\partial \omega}\right)^2\right] \tag{2.28}$$

Conservation of Mean Species Mass

$$\frac{\partial f_{12}}{\partial z} = \left[\omega\left(\frac{d\ln\psi_\infty}{dz}\right)\right]\frac{\partial f_{12}}{\partial \omega} + \frac{\partial}{\partial \omega}\left[\left(D_{2_F}^{\ell} + \frac{C_\mu k^2}{\varepsilon \sigma_f}\right)\frac{\rho^2 u r^2}{\psi_\infty^2}\frac{\partial f_{12}}{\partial \omega}\right]$$
$$+ \frac{\partial}{\partial \omega}\left[\left(D_1^{\ell} - D_2^{\ell}\right)\frac{\rho^2 u r^2}{\psi_\infty^2}\frac{\partial F_1}{\partial r}\right] \tag{2.29}$$

$$\frac{\partial F_4}{\partial z} = \left[\omega\left(\frac{d\ln\psi_\infty}{dz}\right)\right]\frac{\partial F_4}{\partial \omega} + \frac{\partial}{\partial \omega}\left[\left(D_4^{\ell} + \frac{C_\mu k^2}{\varepsilon \sigma_f}\right)\frac{\rho^2 u r^2}{\psi_\infty^2}\frac{\partial F_4}{\partial \omega}\right] \qquad (2.30)$$

Conservation of Mean Square Turbulent Fluctuations in f_{12}

$$\frac{\partial G_{12}}{\partial z} = \left[\omega\left(\frac{d\ln\psi_\infty}{dz}\right)\right]\frac{\partial G_{12}}{\partial \omega} + \frac{\partial}{\partial \omega}\left[\left(D_2^{\ell} + \frac{C_\mu k^2}{\varepsilon \sigma_f}\right)\frac{\rho^2 u r^2}{\psi_\infty^2}\frac{\partial G_{12}}{\partial \omega}\right]$$
$$- \left(\frac{C_f \varepsilon}{\rho u k}\right) G_{12} + \left[\frac{C_G \rho^2 u r^2 k^2}{\varepsilon \psi_\infty^2}\left(\frac{\partial f_{12}}{\partial \omega}\right)^2\right] \qquad (2.31)$$

Conservation of Energy

$$\frac{\partial h}{\partial z} = \left[\omega\left(\frac{d\ln\psi_\infty}{dz}\right)\right]\frac{\partial h}{\partial \omega} + \frac{\partial}{\partial \omega}\left[\left(\lambda_{\ell} + \frac{C_\mu \rho k^2}{\varepsilon \sigma_h}\right)\frac{\rho u r^2}{\psi_\infty^2}\frac{\partial h}{\partial \omega}\right]$$
$$- \frac{2}{3}\left[\left(\frac{\partial k}{\partial z} + k\frac{\partial \ln\rho}{\partial z}\right) - \left\{\omega\left(\frac{d\ln\psi_\infty}{\partial z}\right)\right\}\left(\frac{\partial k}{\partial \omega} + k\frac{\partial \ln\rho}{\partial \omega}\right)\right]$$
$$+ \frac{2}{9\rho}\frac{\partial}{\partial \omega}\left[\frac{C_\mu u r^2}{\varepsilon \psi_\infty^2 \sigma_p}\frac{\partial(\rho k)^3}{\partial \omega}\right] + \frac{1}{\rho}\frac{d\Pi}{dz} + \frac{\varepsilon}{u}$$
$$+ \left[\frac{\mu_{\ell} \rho u r^2}{\psi_\infty^2}\left(\frac{\partial u}{\partial \omega}\right)^2\right] + \left(\frac{S_r}{\rho u}\right) \qquad (2.32)$$

The equation of state relationships are unchanged from those of Eqs. (2.15) - (2.17). However, we now have two additional relationships given by

$$r(\omega, z) = \left[2\psi_\infty(z)\int_0^{\omega}\frac{d\xi}{\rho u}\right]^{1/2} \quad \text{and} \qquad (2.33)$$

$$\frac{d\psi_\infty}{dz} \cong r_\infty(\rho u \mu z)^{1/2} \qquad (2.34)$$

where $\mu = \mu_{\ell} + \mu_t$.

2.2.2 The Boundary and Initial Conditions

The I.C.'s become

$$\phi(\omega, z_0) = \phi_0(\omega) \qquad 0 \leq \omega \leq 1 \tag{2.35}$$

where ϕ, ϕ_0 represent any of the variables except that

$$\psi_\infty(z_0) = \int_0^{R_0} \rho(r, z_0)\, u(r, z_0)\, r\, dr \tag{2.36}$$

The B.C.'s at the edge of the jet become

$$\phi(1, z) = \phi_\infty(z) \qquad z \geq z_0 \tag{2.37}$$

The B.C.'s at the centerline ($r, \omega = 0$) are somewhat different in that it is more convenient to use derived conditions which incorporate Eq. (2.19). They become:

$$\frac{\partial u}{\partial z} = \frac{\partial}{\partial \omega}\left[\left(\mu_\ell + \frac{C_\mu \rho k^2}{\varepsilon}\right) \frac{\rho u r^2}{\psi_\infty^2} \frac{\partial u}{\partial \omega}\right] - \frac{1}{\rho u} \frac{d\Pi}{dz} \tag{2.38a}$$

$$\frac{\partial k}{\partial z} = \frac{\partial}{\partial \omega}\left[\left(\frac{5\mu_\ell}{3} + \frac{C_\mu \rho k^2}{\varepsilon \sigma_k}\right) \frac{\rho u r^2}{\psi_\infty^2} \frac{\partial k}{\partial \omega}\right] + \frac{2}{3}\left[\frac{\partial \ln \rho}{\partial z} + \frac{\partial}{\partial \omega}\left(\frac{\mu_\ell \rho u r^2}{\psi_\infty^2} \frac{\partial \ln \rho}{\partial \omega}\right)\right] k - \frac{\varepsilon}{u} \tag{2.38b}$$

$$\frac{\partial \varepsilon}{\partial z} = \rho \frac{\partial}{\partial \omega}\left[\left(\mu_\ell + \frac{C_\mu \rho k^2}{\varepsilon \sigma_\varepsilon}\right) \frac{u r^2}{\psi_\infty^2} \frac{\partial \varepsilon}{\partial \omega}\right] + \frac{1}{3}\left(\frac{\partial \ln \rho}{\partial z}\right) \varepsilon - \left(\frac{C_2}{uk}\right) \varepsilon^2 \tag{2.38c}$$

$$\frac{\partial f_{12}}{\partial z} = \frac{\partial}{\partial \omega}\left[\left(D_2^\ell + \frac{C_\mu k^2}{\varepsilon \sigma_f}\right) \frac{\rho^2 u r^2}{\psi_\infty^2} \frac{\partial f_{12}}{\partial \omega}\right] + \frac{\partial}{\partial \omega}\left[(D_1^\ell - D_2^\ell) \frac{\rho^2 u r^2}{\psi_\infty^2} \frac{\partial F_1}{\partial \omega}\right] \tag{2.38d}$$

$$\frac{\partial F_4}{\partial z} = \frac{\partial}{\partial \omega}\left[\left(D_4^{\ell} + \frac{C_\mu k^2}{\varepsilon \sigma_f}\right) \frac{\rho^2 u r^2}{\psi_\infty^2} \frac{\partial F_4}{\partial \omega}\right] \tag{2.38e}$$

$$\frac{\partial F_5}{\partial z} = \frac{\partial}{\partial \omega}\left[\left(D_5^{\ell} + \frac{C_\mu k^2}{\varepsilon \sigma_f}\right) \frac{\rho^2 u r^2}{\psi_\infty^2} \frac{\partial F_5}{\partial \omega}\right] + \frac{1}{\rho u}\left(\frac{dF_5}{dt}\right)_{chem} \tag{2.38f}$$

$$\frac{\partial G_{12}}{\partial z} = \frac{\partial}{\partial \omega}\left[\left(D_2^{\ell} + \frac{C_\mu k^2}{\varepsilon \sigma_f}\right) \frac{\rho^2 u r^2}{\psi_\infty^2} \frac{\partial G_{12}}{\partial \omega}\right] - \left(\frac{C_f \varepsilon}{\rho u k}\right) G_{12} \tag{2.38g}$$

$$\frac{\partial h}{\partial z} = \frac{\partial}{\partial \omega}\left[\left(\lambda_{\ell} + \frac{C_\mu \rho k^2}{\varepsilon \sigma_h}\right) \frac{\rho u r^2}{\psi_\infty^2} \frac{\partial h}{\partial \omega}\right] - \frac{2}{3}\left[\frac{\partial k}{\partial z} + k \frac{\partial \ln \rho}{\partial z}\right]$$
$$+ \frac{2}{9}\left\{\frac{1}{\rho} \frac{\partial}{\partial \omega}\left[\frac{C_\mu u r^2}{\psi_\infty^2 \varepsilon \sigma_p} \frac{\partial (\rho k)^3}{\partial \omega}\right]\right\} + \frac{1}{\rho} \frac{d\Pi}{dz} + \frac{\varepsilon}{u} + \frac{S_r}{\rho u} \tag{2.38h}$$

2.2.3 Nondimensionalization

We shall not reproduce the equations here in non-dimensional form since they are virtually a restatement of the above equations in different notation. The parameters were non-dimensionalized by defining:

$$\bar{z} = \frac{z}{R_0}, \quad \bar{u} = \frac{u}{V_0}, \quad \bar{k} = \frac{k}{V_0^2}, \quad \bar{\rho} = \frac{\rho}{\rho_0}, \quad \bar{r} = \frac{r}{R_0}, \quad \bar{\Pi} = \frac{\Pi}{\rho_0 V_0^2},$$

$$\bar{\psi}_\infty = \frac{\psi_\infty}{\rho_0 V_0 R_0^2}, \quad \bar{h} = \frac{h}{h_0}, \quad \bar{\varepsilon} = \frac{\varepsilon \rho_0 R_0^2}{\mu_{\ell_0} V_0^2}, \quad \bar{\mu}_{\ell} = \frac{\mu_{\ell}}{\mu_{\ell_0}}, \quad \bar{S}_r = \frac{S_r}{\rho_0 V_0 h_0},$$

$$\bar{Re}_t = \frac{Re_t}{R_{e_0}^2}, \quad R_{e_0} = \frac{\rho_0 V_0 R_0}{\mu_{\ell_0}}$$

where

R_0 = radius of jet stream at z_0

V_0 = centerline velocity of jet stream at z_0

ρ_0 = density of the jet stream at rest at z_0

μ_{ℓ_0} = dynamic viscosity of the jet stream at rest at z_0

h_0 = total stagnation enthalpy of jet stream at z_0

2.3 FINITE DIFFERENCE FORM

The complete set of difference equations will appear in the topical report previously mentioned so we shall only indicate here the difference methods used.

Our general differential equation takes the form

$$\frac{\partial \phi}{\partial z} = a \frac{\partial \phi}{\partial \omega} + \frac{\partial}{\partial \omega}\left[b \frac{\partial \phi}{\partial \omega} \right] + c\phi + d\phi^2 + e \tag{2.39}$$

where a, b, c, d, and e are coefficients which are functions of all of the parameters of the problem (all of the ϕ's).

Let us denote $\phi(\omega_i, z_n)$ by ϕ_i^n. We can denote two different values of $\phi(\omega_i, z_{n+1})$ by ϕ_i^{n+1} and $\phi_{i,0}^{n+1}$ where the former is the unknown value to be determined and the latter is the best guess to the unknown (usually the result of a previous iteration). Let us also define α, β such that they are constants with $1/2 \leq (\alpha, \beta) \leq 1$ and α may or may not equal β. Then we get that:

$$\frac{\partial \phi}{\partial z} = \frac{\phi_i^{n+1} - \phi_i^n}{\Delta z} \tag{2.40a}$$

$$a \frac{\partial \phi}{\partial \omega} = \left[\beta a_i^{n+1} + (1-\beta) a_i^n \right] \left[\alpha \left(\frac{\phi_{i+1}^{n+1} - \phi_{i-1}^{n+1}}{\omega_{i+1} - \omega_{i-1}} \right) + (1-\alpha) \left(\frac{\phi_{i+1}^{n} - \phi_{i-1}^{n}}{\omega_{i+1} - \omega_{i-1}} \right) \right] \tag{2.40b}$$

$$\begin{aligned} \frac{\partial}{\partial \omega}\left[b \frac{\partial \phi}{\partial \omega} \right] = & \left[\left\{ \beta (b_{i+1}^{n+1} + b_i^{n+1}) + (1-\beta)(b_{i+1}^{n} + b_i^{n}) \right\} \right. \\ & \left\{ \frac{\alpha(\phi_{i+1}^{n+1} - \phi_i^{n+1}) + (1-\alpha)(\phi_{i+1}^{n} - \phi_i^{n})}{(\omega_{i+1} - \omega_i)(\omega_{i+1} - \omega_{i-1})} \right\} - \left\{ \beta (b_i^{n+1} + b_{i-1}^{n+1}) \right. \\ & \left. \left. + (1-\beta)(b_i^{n} + b_{i-1}^{n}) \right\} \left\{ \frac{\alpha(\phi_i^{n+1} - \phi_{i-1}^{n+1}) + (1-\alpha)(\phi_i^{n} - \phi_{i-1}^{n})}{(\omega_i - \omega_{i-1})(\omega_{i+1} - \omega_{i-1})} \right\} \right] \end{aligned} \tag{2.40c}$$

$$C\phi = \left[\beta C_i^{n+1} + (1-\beta)C_i^n\right]\left[\alpha\phi_i^{n+1} + (1-\alpha)\phi_i^n\right] \tag{2.40d}$$

$$d\phi^2 = \left[\beta d_i^{n+1} + (1-\beta)d_i^n\right]\left[\alpha\left\{2\phi_{i,0}^{n+1}\,\phi_i^{n+1} - \left(\phi_{i,0}^{n+1}\right)^2\right\} + (1-\alpha)\left(\phi_i^n\right)^2\right] \tag{2.40e}$$

$$e = \beta e_i^{n+1} + (1-\beta)e_i^n \tag{2.40f}$$

When the forms of Eqs. (2.40) are applied to the equations of motion, we can collect terms as coefficients of ϕ_{i-1}^{n+1}, ϕ_i^{n+1}, ϕ_{i+1}^{n+1} and all the other terms independent of those three quantities (note that a_j^{n+1}, b_j^{n+1}, c_j^{n+1}, d_j^{n+1}, and e_j^{n+1} are all evaluated using $\phi_{j,0}^{n+1}$ if it is needed). Thus, we have a resulting finite difference equation of the form

$$A\phi_{i+1}^{n+1} + B\phi_i^{n+1} + C\phi_{i-1}^{n+1} = D \tag{2.41}$$

which is the classical tridiagonal form which can be easily solved by standard methods.

III. EQUATION OF STATE

Relationships between thermodynamic quantities are required if the flame equations are to be solved. In general, two such relationships are required: The "thermal and caloric equations of state" which relate the temperature, volume, enthalpy and pressure of systems which are also changing in composition.

The "thermal" equation of state requirement is readily satisfied with an ideal gas formulation based upon chemical equilibrium.

Provision of a "caloric" equation of state relationship requires, as an initial step, that numerical fits be created for the heat capacity, enthalpy, and entropy for each of the species deemed present at chemical equilibrium. In most cases, these numerical fits were already in existence at Systems, Science and Software. (They are based on JANNAF thermochemical data.) Additional numerical fits were established as needed and all fits were checked for accuracy over the domain of interest. These data will be included in the write-up of the computer code to be published as part of the contractual work.

The FCHEM computer subroutine was next established. This routine assumes that the flame system is at approximately one atmosphere pressure and requires as input the total enthalpy of the system and the mass fractions of fuel, oxidant, diluent, and products. These mass fractions are broken down into the elemental quantities, in moles per gram of mixture and, from these, a set of chemical equilibrium species is assembled, at the specified enthalpy. These concentrations are then used to calculate the adiabatic flame temperature and the PV product. (The latter quantity is determined from the flame temperature and the ideal gas law.)

Calculations are greatly simplified by the fact that, at equilibrium, the concentration of fuel is negligible if oxidant is in excess, or vice versa. (The mass fraction of fuel which may be converted to soot is generally on the order of milligrams per gram of fuel, and can be neglected here.) Further, at ordinary diffusion flame temperatures, certain dissociation reactions, e.g.,

$$H_2O \rightleftharpoons H + OH$$

can be neglected. The only chemical equilibrium which must be included is the water gas reaction:

$$CO_2 + H_2 \rightleftharpoons H_2O + CO.$$

Even this equilibrium may be neglected in lean flames.

Elemental composition is determined by assuming that combustion products do not separate (i.e., they travel downstream together). The formula of the fuel thus gives the ratio of CO_2 to H_2O.

From the elemental composition and stoichiometry, an initial estimate is made of the position of equilibrium. Since there is no change in the number of moles of gas in the water gas reaction, there is no dependence of the position of equilibrium on the system pressure and it is not required as input to find the position of equilibrium. Using "E" and "S" to denote final equilibrium and starting estimates, the law of mass action gives:

$$K_{EQ} = \frac{[E_{H_2O}][E_{CO}]}{[E_{CO_2}][E_{H_2}]} = \frac{[S_{H_2O}+\delta][S_{CO}+\delta]}{[S_{CO_2}-\delta][S_{H_2}-\delta]} \qquad (3.1)$$

where the square brackets denote concentrations in moles per gram of mixture; K_{EQ} is the equilibrium constant for the water-gas reaction, and is a function of temperature, and δ

is the change in concentration from the starting estimate to the final equilibrium value. This equation is a quadratic in δ which can thus be readily computed without iteration.

As both the enthalpy and the equilibrium constant are non-trivial functions of temperature, it is necessary to iterate for self-consistency between enthalpy, T, and the equilibrium position. Successive estimates of T are determined from the equilibrium mixture heat capacity at the previously estimated T:

$$T_{(n+1)} = T_{(n)} + [h_{input} - h_{(n)}]/[C_p(T_n)] \qquad (3.2)$$

where the subscript in parentheses denotes iteration stage. Three iterations ordinarily suffice to reach a self-consistent solution.

IV. THE SOOT MODEL

The presence of soot in flames depends primarily upon the type of fuel involved and the amount and rate of mixing of fuel and oxidant.

Certain flames are automatically soot free because the fuel contains no carbon. In addition, many hydrocarbon or carbon based fuels (e.g., LNG and methanol) also can give soot free flames when the fuel-oxidant ratios are within certain concentration domains throughout the flame. Other carbon based flames (e.g., acetylene) are commonly smoky or sooty.

Even when a flame is characterized as sooty, relatively small amounts of carbon are involved. For example, a very smoky flame produced from jet engine fuel (e.g., JPY) may involve a mass ratio of solid carbon to fuel of approximately 0.5 percent. (The usual soot to fuel mass ratio is a factor of fifty smaller.) Thus, only negligible changes in the combustion heat release and gas equation of state will result, although substantial changes may occur in the absorption and scattering of visible light and infrared radiation.

The amount of soot present in flames must result from the balancing of two factors: The rates of soot particle formation and growth, and the rate of oxidation of soot. Relevant data about these factors can be obtained from 1) studies on laboratory flames and similar combustion processes, and 2) examination of the details of the chemical kinetics for the processes which are believed to be involved.

Current knowledge of the detailed chemical processes which lead to the formation of soot is very incomplete. Qualitative understanding of these processes can provide guidance in the formulation of a mathematical model. Estimates of the parameters can then be gained from experimental studies.

Lee, Thring, and Beer[5] and Thring, Beer, and Foster[6] have determined that soot particles can be formed initially in less than a millisecond, much less than the residence time of soot in a large flame. (They show that the total soot concentration appears unaffected by substantial variations in residence time, preheating of combustion air, or variations in the fuel-oxidant mixing rate.) This suggests that the initial precipitation of soot particles is the dominant process, rather than their subsequent growth in fuel-rich regions of the flame.

The experimental study of Ref. 7 confirms the appearance of soot within one millisecond of the initial combusion reactions with both unsaturated and saturated hydrocarbon fuels. References 8 and 9 also present data which support the conclusion that the particle distribution in flames is hardly influenced by scale effects* and the residence time in the flame.

Porter,[10] in his theorization about carbon black formation in flames, suggests that C_2H_2 is the last chemical stage before carbon formation. Experimental work confirms this, showing that the carbon black concentration curve begins to rise markedly when the C_2H_2 concentration decreases; rather than at the earlier (upstream) positions at which C_2H_2 and C_2H_6 disappear in a natural gas flame (Ref. 8).

Hein[11] has recently done an extensive study of fuel oil and propane flames with varying amounts of premixing of fuel and oxidant. The assumption that the mass of soot formed is first order in time and per mass of hydrocarbon available

*They find a mean particle size of 230 Å with a size range of 100 - 400 Å. These values for 8 meter (about 26 1/4 feet) flames are quite close to those found by Tesner [12] for small flames and by Maraval [9] for fuel oil and natural gas diffusion flames.

leads to an expression of the form:

$$\left(\frac{dm}{dt}\right) = [\text{hydrocarbon}]\ A\ e^{-E_F/RT} \qquad (4.1)$$

in which [hydrocarbon] is the concentration of unburned hydrocarbons, $E_F \approx 21\text{-}22$ kcal/g-mole and $A \approx 10^8$. This expression fits the data well for soot production in slightly premixed, turbulent propane flames and has been adopted for use in this study.

At the tail end of the flame, measured soot burnout rates were shown[6] to be comparable to those observed in laminar laboratory flame studies. The specific oxidation rate was found to be correlated by:

$$\left(\frac{dm}{dt}\right) = 1.085 \times 10^4\ P_{O_2}\ T^{-1/2}\ e^{-39300/RT}, \qquad (4.2)$$

for various partial pressure or oxygen ($0.04 \leq P_{O_2} \leq 0.1$ atm) and temperatures ($1300 \leq T \leq 1700$ k).

Reference 12 also suggests a first order dependence of (dm/dt) on P_{O_2}, and an activation energy close to 40 kcal/mole.

Fenimore and Jones[13] have argued that soot oxidation is only weakly dependent on oxygen concentration.

References 14 and 15 in careful reviews of these and other studies suggest that the correlation formula of Ref. 16 provides a reasonable explanation for all published soot oxidation data. We have adopted this formulation and will use the best-fit parameters provided by Ref. 15.

The equation adopted for the specific surface soot oxidation rate is:

$$\left(\frac{dm}{dt}\right) = 12\left\{\left(\frac{k_a P_{O_2}}{1 + k_z P}\right) \xi + k_B P_{O_2}(1-\xi)\right\} \qquad (4.3)$$

where

$$\xi \equiv \{1 + k_T/(k_B P_{O_2})\}^{-1}$$

and

$$k_A = 20\ e^{-15100/RT}$$

$$k_B = 4.46 \times 10^{-3}\ e^{-7640/RT}$$

$$k_T = 1.51 \times 10^{-5}\ e^{-48800/RT}$$

$$k_Z = 21.3\ e^{2060/RT}$$

V. RADIATION TRANSPORT

5.1 CALCULATION OF DESIRED RADIATION QUANTITIES

In the equation which describes the conservation of energy in a reacting, radiating flow, the divergence of the radiative flux appears explicitly and physically represents the net rate of loss (or gain) of radiant energy per unit of volume. This can be expressed as[17]

$$D(r) = \int_0^\infty \left\{ k_\nu \left[4\pi B_\nu(\vec{r}) - G(\vec{r}) \right] \right\} d\nu \qquad (5.1)$$

where the spectral incident radiant energy is defined as

$$G_\nu(\vec{r}) = \int_0^{2\pi} \int_{-1}^{+1} I'_\nu(r,\mu,\phi)\, d\mu\, d\phi \qquad (5.2)$$

The first term on the right hand side of Eq. (5.1) represents emission and the second term accounts for absorption of radiant energy. The radiation heating rate, $\dot{\Pi}$, is defined as

$$\dot{\Pi}(\vec{r}) = \frac{-1}{\rho C_p} D(\vec{r}) \qquad (5.3)$$

Note that the volume element to be heated can be anywhere (i.e., inside or outside the flame). To evaluate the heating rate one needs to know the appropriate local properties and the radiation field as these appear in Eqs. (5.1) through (5.3).

The radiant field as well as the medium properties can be obtained as discussed in Section 5.3 and 5.4. It is mentioned there that to solve the equation of radiation transport is a formidable task and that some approximations must be made to obtain the solution with a reasonable computer

time. These approximations should be consistent with the uncertainties in other input data as well as the desired accuracy of the solution.

It should be pointed out that approximations made to evaluate the radiant heating rate inside the fire should be consistent with other modes of heat transfer. At locations in the fire at which radiation is an important mode of heating, greater accuracy is desired than for those locations at which the radiant heating forms only a small fraction of the total heating rate.

The kind of approximation to be made and solution approaches to be taken to obtain the radiation quantities depends on the specific problem. In our problem for example, a Rosseland or diffusion approximation for radiation transport could be more suited inside an optically thick flame like that of benzene but may not be a good approximation for a methanol flame which produces little soot. Different approximations may also be better suited to different regions of the plume.

5.2 EQUATION OF RADIATION TRANSPORT

The equation relating the change in specific intensity of radiation at frequency ν along the line of site[18] is given by

$$\frac{dI_\nu(s,\Omega)}{ds} = -\beta_\nu I_\nu(s,\Omega) + k_\nu B_\nu(T) - \frac{\sigma_\nu}{4\pi}\int_{\Omega=4\pi} I_\nu(s,\Omega')p\,(\Omega',\Omega)d\Omega' \qquad (5.4)$$

where σ_ν and β_ν $(=k_\nu+\sigma_\nu)$ are the spectral scattering and attenuation coefficients, respectively, and p_ν is the scattering or phase function. The first term on the right hand side accounts for the extinction (absorption + scattering) of radiant energy. The second and third terms represent the contributions to the intensity by emission and scattering from the elemental volume, In the writing of Eq. (5.4) the term $(1/c)(\partial I_\nu/\partial t)$ has been neglected because the velocity of light c is large and hence this term is negligible[19] in comparison with others.

To solve for the intensity of spectral radiation inside or outside the plume, knowledge of k_ν, β_ν, B_ν, p, and T as well as any radiation incident on the boundary of the plume from external sources is required. Once the transport equation is solved for the spectral intensity of radiation, the quantity of interest, the divergence of the flux or the radiation heating rate, can be easily determined from Eqs. (5.1) and (5.3), where the quantity inside the integral yields the spectral divergence at frequency ν.

In problems such as this, there are two difficulties in obtaining I_ν. First, the shape of the plume, the local plume pressure, the temperature, the concentration of species, and the size distribution of particles as well as

their spectral properties are not known accurately. Second, even if these are known, it is impossible to solve the equation of transport, Eq. (5.4), for completely arbitrary conditions.

5.3 FORMAL SOLUTION OF THE EQUATION OF TRANSPORT

Formal solution of Eq. (5.4) can be written as[17]

$$I(\tau(s),\Omega) = I_b(\tau_b,\Omega)\exp(-(\tau_b-\tau)) + \int_{\tau}^{\tau_b} S(\tau',\Omega)\exp(-(\tau'-\tau))d\tau' \qquad (5.5)$$

where I_b is the intensity of radiation incident at the boundary, as shown in Fig. 5.1, and the optical thickness τ between two locations is given by the band models chosen. In the just-overlapping-line approximation, the optical thickness between two locations s_1 and s_2 is defined as

$$\tau_{s_1-s_2} = \int_{s_1}^{s_2} (k+\sigma)ds \qquad (5.6)$$

The source function is defined as

$$S_\nu(\tau,\Omega) = \left(1 - \frac{\sigma_\nu}{\beta_\nu} B_\nu(\tau)\right) + \frac{\sigma_\nu}{\beta_\nu} H_\nu(\tau,\Omega) \qquad (5.7)$$

where

$$H_\nu = \frac{1}{4\pi} \int_{\Omega'=4\pi} p_\nu(\Omega',') I_\nu(\Omega')d\Omega' \qquad (5.8)$$

The ratio of scattering coefficient and extinction coefficient is termed as albedo and sometimes denoted by ω (i.e., σ/β). It is called the albedo for single scattering in the radiative transfer literature,[19] and Schuster number[17] in the Russian Engineering literature.

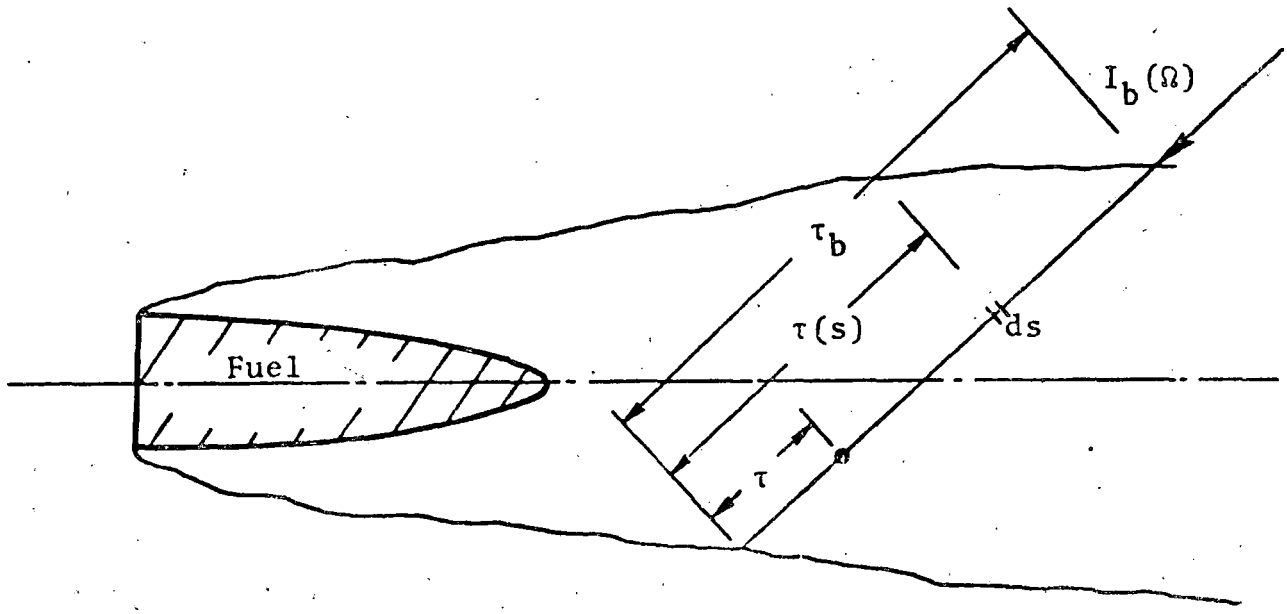

Figure 5.1. Schematic representation of torch fire.

In the preceding paragraph we have assumed that the source function $S(\tau,\Omega)$ is known. As a matter of fact it is not, and Eqs. (5.5) and (5.7) do not provide practical solutions to the equation of transfer. Important approximations under which solutions have been obtained are discussed below briefly.

5.3.1 Schuster-Schwarzschild Approximation

For isotropic scattering $p(\Omega',\Omega)= 1$, the equation of radiative transfer can be written as

$$\frac{dI_\nu(s,\Omega)}{ds} = - \beta_\nu I_\nu(s,\Omega) + k_\nu B_\nu(T)$$

$$+ \frac{\sigma_\nu}{4\pi} \int_{\Omega=4\pi} I_\nu(s,\Omega')d\Omega' \qquad (5.9)$$

Schuster[20] and Schwartzschild[21] have divided the radiation field into the forward $\Omega=0$ to 2π and the backward $\Omega=2\pi$ to 4π stream of mean intensities I^+ and I^-, respectively. Mathematically these are the arithmetic means of $I(\tau,\Omega)$ over the respective forward and backward hemispheres. The mean intensities are defined as

$$I^+ = \frac{1}{2\pi} \int_{\Omega=0\to 2\pi} I(\Omega')d\Omega' \qquad (5.10)$$

and

$$I^- = \frac{1}{2\pi} \int_{\Omega=2\pi\to 4\pi} I(\Omega')d\Omega' \qquad (5.11)$$

Integration of Eq. (5.9) over the forward and backward hemispheres[17] yields two differential equations which can be solved. A number of investigators[22-23] have employed this approximation to plane parallel geometries with some success in radiation transfer problems.

5.3.2 Milne-Eddington Approximation

The Milne-Eddington approximation has been used for the one-dimensional infinite slab geometry in a number of problems. This approximation again assumes that scattering function is isotropic, i.e., $p(\Omega',\Omega)\equiv 1$. The details are omitted and can be found elsewhere.[24-25] This approximation has been used for the one-dimensional infinite slab geometry in a number of problems.[26-27]

5.3.3 The Spherical Harmonics Method

In this method the solution of equation of transfer is sought in the form of an expansion of $I(\tau,\mu)$ in a series of Legendre polynomials $P_n(\mu)$. These polynomials form a complete set of orthogonal functions in the interval $-1 \leq \mu \leq 1$. The mathematical details of the method are given, for example, by Kourganoff[28] for the one-dimensional slab and by Davison[29] for other geometries.

5.3.4 The Discrete Coordinate Method

The Schuster-Schwarzschild approximation is really a very primitive form of the discrete coordinate method. The basis of this method is to divide the radiation flux into more than just two streams. In this method the radiation field $I(\tau,\mu)$ is divided into $2n$ streams in the directions $\mu_i (i = \pm 1, \pm 2 \ldots \pm n)$. Once the cocrdinates μ_i are chosen more or less regularly in the interval $-1 < \mu < 1$ the equation of transfer can be replaced by a system of $2n$

differential equations. Additional details can be found in Refs.18,28. It has also been recently used in the form of four and six flux models to approximate the radiation transport in furnace problems.[30-31]

5.3.5 The Long Characteristics Approach

In cases where scattering is negligible ($\sigma \lesssim 0$), or the energy once scattered is ignored, the last term in Eq. (5.4) can be dropped and the integro-differential equation reduces to a differential equation. The same result is obtained when the phase function is highly peaked in the forward direction[32] and hence can be represented by a delta function, i.e.,

$$p(\Omega,\Omega') = 1 \quad \text{for} \quad \Omega = \Omega'$$

$$= 0 \quad \text{for} \quad \Omega \neq \Omega'$$

The last term in Eq. (5.4) reduces to $\sigma_\nu I_\nu(s,\Omega)$. When it is combined with the first term on the right side of the equation, it yields $-k_\nu I_\nu(s,\Omega)$. This assumption considerably reduces the computational effort.

Under the assumption that radiation once scattered is lost from the system, Eq. (5.4) reduces to

$$\frac{dI_\nu(s,\Omega)}{ds} = -\beta_\nu I_\nu(s,\Omega) + k_\nu B_\nu(T). \tag{5.12}$$

The solution to this equation for the intensity of radiation emerging at location τ is

$$I_\nu(\tau,\Omega) = I_\nu(\tau_b,\Omega)\exp\left(-(\tau_b-\tau)\exp\left(-(\tau_{b,sc}-\tau_{sc})\right)\right) + \int_\tau^{\tau_b} B_\nu(T)\exp\left(-(\tau'-\tau)\exp\left(-(\tau'_{sc}-\tau_{sc})\right)\right)d\tau' \tag{5.13}$$

where $I_\nu(\tau_b,\Omega)$ is the intensity of external radiation incident onto the plume. The first term on the right hand side is the radiation arriving at the point of interest which has only been attenuated by the plume (absorbed + scattered). Note that I_ν is the intensity incident onto the outside of the plume (plume boundary). The second term represents the net emission due to the emitting, absorbing and scattering species of the plume where $B_\nu(T)$ is the blackbody emission term corresponding to temperature T at location τ'. Note that in this equation optical inhomogeneities (solid particles, liquid droplets, etc.) make two kinds of contribution. One, because these are absorbing/emitting, they effect the absorption coefficient of the plume and its effect is no different than those of the other species in the plume such as H_2O, CO_2. This contribution is included in Eq. (5.13) while calculating the values of τ and the necessary input data (the absorption coefficient) for this is provided by Mie calculations. Second, because unlike other species in this problem, the optical inhomogeneities also scatter, this is taken into account by introducing τ_{sc} in Eq. (4.13). The optical thickness due to scattering can be calculated from the data provided by Mie theory, and evaluation of τ_{sc} is similar to that of τ. Note that when there are no optical inhomogeneities or scattering centers, the optical thickness τ_{sc} becomes zero, $\exp(-\tau_{sc}) = 1$ and the equations reduce further to

$$I_\nu(\tau,\Omega) - I_\nu(\tau_b,\Omega) \exp(-(\tau_b-\tau)) + \int_\tau^{\tau_b} B_\nu(T) \exp(-(\tau'-\tau))d\tau' \qquad (5.14)$$

S^3 intends to follow the long characteristics approach for calculation of radiative quantities rather than the six

flux model. Although this approach is tedious, it is expected to be more accurate for this kind of problem. The long characteristics approach can easily take into account the spectral absorption and scattering properties of the constituents as well as the effect of temperature, pressure and concentration gradients. This capability of the S^3 code is demonstrated in results shown in Fig. 5.2 where the spectral optical thickness and transmittance is plotted for a typical line of sight through the fire plume such as shown in Fig. 5.1. These results correspond to a plume which consists principally of two emitting and absorbing species, CO_2 and H_2O with mole fractions of 0.04 and 0.06, respectively, at the exit plane and at a temperature of nearly 1400 R. The temperature, pressure and concentration of species varies with location. Although these results are not for a real torch fire, these do demonstrate that radiation properties of H_2O vapor and CO_2 are highly wavelength dependent. The plume along the same line of sight can be optically thin and optically thick, depending upon the wavelength. As is discussed later, some of the band model approximations which are valid for the spectrum for which the plume is optically thin may not be valid for the spectrum in which the plume is not optically thin.

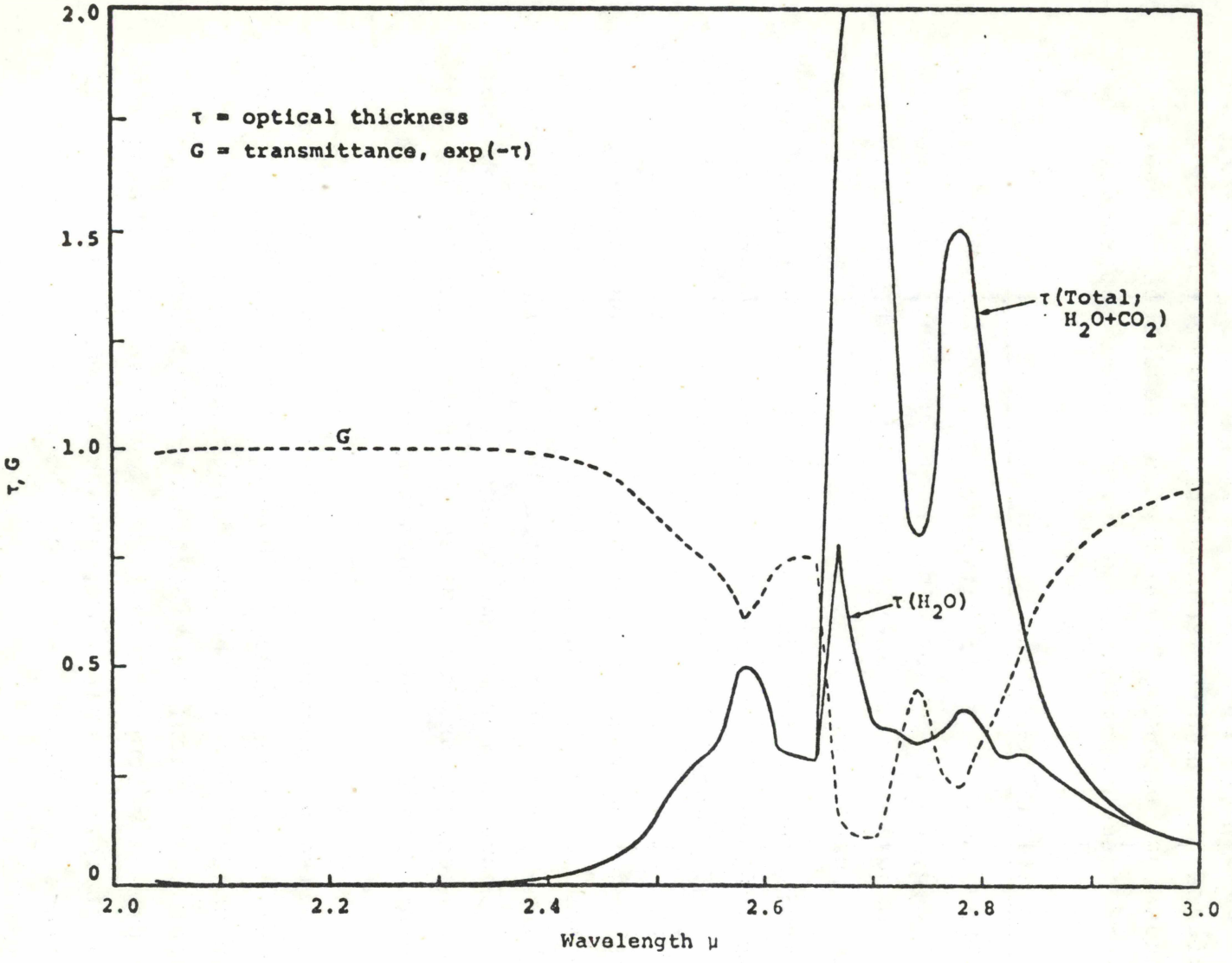

Figure 5.2. Optical thickness and transmittance of the plume versus wavelength for a typical line of sight.[ ]

5.4 RADIATION PROPERTIES OF CONSTITUENTS

Solution of the radiation transport Eq. (5.4), requires knowledge of the radiation properties, the absorption coefficients k_ν and the scattering cross sections σ_ν. For discussion purposes, it is logical to discuss the properties of gaseous products and particulates separately.

5.4.1 Radiation Properties of Gaseous Products

The constituents of a fire contain mainly combustion products H_2O, CO_2, CO, air and, in the unburned zone, fuel vapor. (Other products such as NO_x may also be present in negligible quantities.)

It is well known that the absorption coefficient of a gas is influenced not only by its temperature and pressure but by the presence of other species as well. Hence, to predict the absorption coefficient of a mixture of gases, one should not only know the relevant radiation parameters of each species but should also know how to combine these. The problem is further complicated by the species properties gradients found in fires. We assume in this discussion that species concentrations and system property gradients have been computed, and we now discuss the properties of gaseous species.

At fire temperatures, the gaseous species contribution to radiant energy is primarily due to radiation from vibration-rotation bands. Due to the rapid spectral variation of the absorption coefficient in vibration-rotation bands, this feature presents computational difficulties. The absorption coefficient for a single line, broadened principally by collisional processes (which is typical of plume conditions) is given by[34,35]

$$P_\omega = \frac{\gamma}{\pi} \frac{S}{(\omega-\omega_o)^2 + \gamma^2} \qquad (5.15)$$

where we have used $P_\omega (cm^{-1}\ atm^{-1})$ as the spectral absorption coefficient ($k_\omega = P_\omega p$ where p is the pressure), S is the integrated line intensity ($cm^{-2}\ atm^{-1}$), ω_o is the wavenumber at the center of the line and γ is the line half width. For collision broadened lines

$$\gamma = \gamma_o \frac{p}{p_o} \sqrt{\frac{T_o}{T}} \tag{5.16}$$

where the subscript o refers to standard conditions. It can be seen that the dependence on local thermodynamic conditions thus presents one with a spectral absorption coefficient which varies through the plume. Thus a line emitted from the plume is not a simple Lorentzian shape but is distorted by the non-homogeneous path. While this presents no particular difficulties for a single line, the problem is compounded by the fact that the contribution to the absorption coefficient at wavenumber ω represents the contribution of many lines whose tails contribute to the absorption, i.e.,

$$P_\omega = \sum_j \frac{\gamma_J}{\pi} \frac{S_J}{(\omega - \omega_{o,J})^2 + \gamma_J^2} \tag{5.17}$$

where the sum includes the contribution of all lines which have finite absorption at the wavenumber ω.

Much of the above material has been discussed in various textbooks. We have reproduced the essentials here to provide a common ground for further discussion.

Molecular Band Models

It is apparent from Eq. (5.17) that in order to compute the spectral absorption coefficient at a particular wavenumber (wavelength) of interest the contribution of several

hundred lines must be taken into account. Furthermore, this lengthy procedure must be repeated at each wavenumber in order to compute the intensity emitted within a given spectral bandpass. While it is possible to accomplish such a calculation for molecules such as CO_2 and H_2O, it is not expedient or even necessary to do so if one is content with wavelength resolution of greater than about 25 cm^{-1}. Since most instruments used to perform measurements in fact do not possess resolving power of 25 cm^{-1}, it is generally not worthwhile for practical applications to perform such exacting calculations.

A common procedure is to develop molecular band models which hypothesize some form for the distribution of lines, and their widths and strengths, which when applied produces "synthetic spectra" which closely reproduce those actually measured. Without going into all of the mathematical details which are not needed for the present discussion, the following band models have been used for various applications and are discussed extensively in the literature.[34-36]

- Rectangular Box Model
- Just-overlapping-line Model
- Elsasser Band Model
- Mayer-Goody Statistical Model
  - (a) Exponential line probability distribution
  - (b) Inverse power line probability distribution.

Rectangular Box Model

The rectangular box model is the simplest molecular band model and gives the least precise results regarding spectral resolution. This model replaces the complete molecular band by a band whose absorption coefficient is constant over some effective bandwidth.[34]

Just-Overlapping-Line Model

The just-overlapping model is the next step up in sophistication and reproduces the spectral structure of a band reasonably well in most applications. The model, however, is applicable only where the pressure is sufficiently high to "smear out" the rotational structure, i.e., the lines are broadened to such an extent that adjacent lines overlap to produce a relatively smooth variation in spectra.[35] It can be shown that this model is applicable if the line width is of the same order as the line spacing. For plume applications, it can be shown that such conditions are in fact met for CO_2 at pressures of several atmospheres, while somewhat higher pressures are required for the H_2O vapor. Corrections to account for non-complete overlapping have been proposed and have worked successfully in some applications.[35]

Elsasser Band Model

The Elsasser band consists of equally spaced, equally intense lines whose profiles are described adequately by the Lorentx profile, i.e., they are collision broadened, c.f., Eq. (5.15).[34,35] The sum over all contributing lines can be computed semi-analytically for specified line intensities and line spacing. This model has certain disadvantages when attempting to model the absorption in molecules such as H_2O which do not possess regular line spacing. However, the Elsasser model has provided extremely accurate results for CO_2 in all bands of interest for plume calculations, for application to computing emission from hot gases, and for atmospheric transmission calculations.[35-37]

Mayer-Goody Statistical Model

The Mayer-Goody statistical model assumes that a band is composed of lines which are distributed at random throughout

the band and that there is no correlation between the position of a line and its intensity.[37] Once again it is assumed that the lines are Lorentzian. Two common models are used for the distribution function of lines. These are the exponential distribution function and the inverse first power distribution function. It is not clear at this point which of these assumptions is best forthe plume problem. Verification awaits experimental measurements. However, extensive results for atmospheric transmission problems indicate that there is little difference between the two.[37] As we have stated, the statistical model produces excellent results for H_2O and has also been used successfully for CO_2.

Scaling Approximation for Inhomogeneous Applications

None of the band models previously discussed can be applied without modification to account for the inhomogeneous path lengths encountered in a typical fire plume. As we discussed previously, the gradients in thermodynamic variables distort the Lorentzian profile of a line as given by Eq. (5.15). Several methods may be employed for the treatment of this problem and are discussed extensively in the literature.

- Reduction of radiation transport equation to a difference equation in which the continuous distribution of properties is replaced by a set of discrete zones. Each zone is locally homogeneous and direct application of the previous equation is possible.
- Scaling approximations are applied to reduce the inhomogeneous problem to a homogeneous one.[36,37]

(a) One parameter scaling. It is assumed that pressure most strongly affects the resultant transmission and that the absorption coefficient may be expressed as a product of a purely pressure term and a purely frequency dependent term. Accordingly, the inhomogeneous path is replaced by a homogeneous path at some mean pressure, i.e., mean mass of gas.

(b) Two parameter scaling (Curtis-Godson approximation). In the C-G approximation both pressure and temperature effects on line absorption coefficients are taken into account. Consequently, both the temperature variation on line intensity and line width is accounted for. The choice of width and intensity is determined by obtaining the correct absorption in the weak line and in the strong line limit.

As has been indicated above, the C-G approximation, which is the highest order scaling approximation available, is basically applicable only for the weak and strong lines limits (thin or opaque). While the approximation has found a wide degree of acceptance and use for solar transmission through atmospheres (for which extensive experimental data are available) it is not clear that the same conclusion will hold for fire plumes.[37,38] It can be shown for instance, that for the computation of radiative flux in the atmosphere where extremely long path lengths are involved, most bands responsible for atmospheric heating contain a significant fraction of lines which are predominantly optically thick. For this reason, the Curtis-Godson approximation gives results which are correct to within a few percent of exact calculations. The only exception which we have found is for the

9.6 μ band of ozone.[39] In this case, the optical depth of ozone is near unity. Thus, neither the weak line nor strong line assumption is applicable.

It is also worth noting the work of Zdunkowski and Raymond[40] on the degree of spectral resolution obtainable for accurate calculations. They conclude that the C-G approximation gives very accurate results when compared with exact results. Under similar conditions, the effective mass (single parameter scaling approximation) offers no particular advantage. They further state that it is necessary to include within the wavenumber interval under investigation, the effect of line wing contributions from adjacent intervals. They find that for interval sizes large enough to contain numerous lines, the effect of line wings due to the presence disregarded in many cases. A general rule is that 50 to 100 lines must be present within the interval before such neglect can be made safely. This translates to spectral band passes of about 25 cm^{-1} or larger. Operating on this assumption can save significant amounts of computer time.

Selection of band model and scaling approximation for calculating the radiation quantities depends on the accuracy desired, the choice of the solution technique, the radiation property data of the constituents available, etc. For example, to employ the C-G technique, one needs to know not only the intensities with a fine resolution, but line spacings and line widths as well. While this kind of data is available for constituents such as water vapor, carbon dioxide, carbon monoxide, etc., it is not available for fuels. The most detailed data of radiation properties of gaseous fuels, which we have been able to locate, is published by American Petroleum Institute in their publication 44. The data is not in the usable form, i.e., in the form of absorption coefficients. The data is in the form of percent transmittance of a cell

filled with the fuel gas, as shown in Fig. 5.3. To use this data in the calculations one must read the percentage transmittance as a function of wavelength from the curves and then reduce this data to a useable form. It should be mentioned that these curves do not show any data below 2 μ which must be found from other sources. The literature search to obtain the most up to date data on fuels is continuing.

S^3 feels that it has the best available radiation property data needed for H_2O vapor, CO_2 and CO over a wide temperature and wavelength range with good spectral resolution. Table 5.1 shows the numerical values of temperature range, wavelength range and the resolution for which the values of absorption coefficient $\bar{k}$ are available.

5.4.2 Radiation Properties of Solid Particles and Liquid Droplets

Mie Scattering, Single Particle*

The absorption and scattering of radiation from spherical particles can be determined from Mie scattering theory.[41] Mie scattering considers the effect of a forced oscillation of a radiative field upon a spherical particle and the induced fields inside and outside the sphere. These results are derived in Ref. 42, and are summarized below.

Mie scattering of a plane wave of wavelength λ from a particle of radius a is described rigorously by the following infinite series:

$$\sigma_{ext} = \frac{\lambda^2}{2\pi} \sum_{n=1}^{\infty} (2n+1) \text{ Re } (a_n + b_n) \qquad (5.18)$$

*The nomenclature in this section is self contained.

TABLE 5.1

RADIATION ABSORPTION PROPERTIES

Constituents	Parameter	Wavenumber Range, cm^{-1}	$\Delta\nu$, cm^{-1}	Temperature Range °K
H_2O	$\overline{\kappa}$	50-11000	25	300-3000
CO_2	$\overline{\kappa}$	500-3750	25	300-3000
CO	$\overline{\kappa}$	1025-2350	25	300-3000

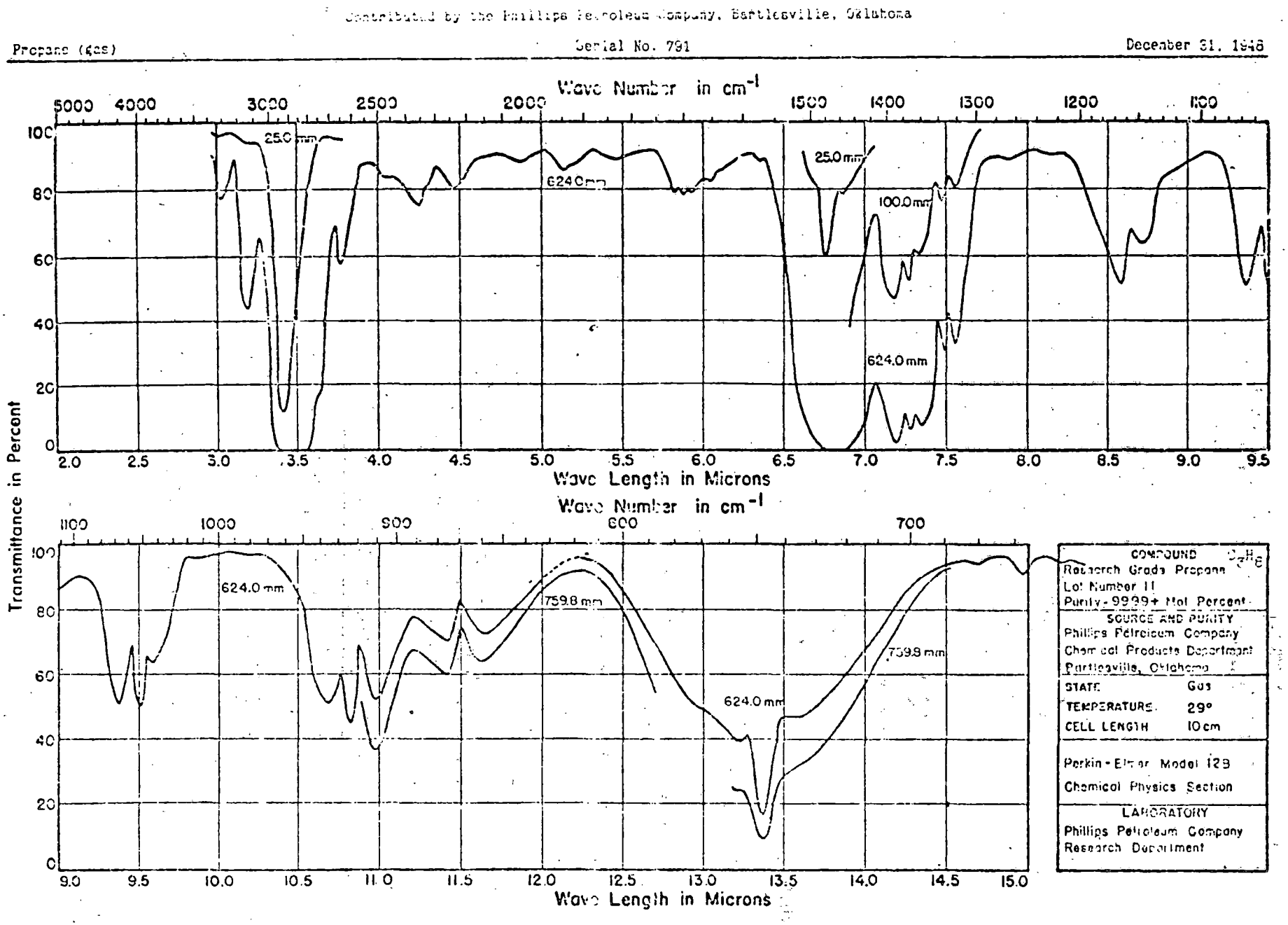

Figure 5.3 Spectral transmittance of propane gas through 10 cm long cell at room temperature.

$$\sigma_{sca} = \frac{\lambda^2}{2\pi} \sum_{n=1}^{\infty} (2n + 1)(|a_n|^2 + |b_n|^2) \qquad (5.19)$$

$$\sigma_{abs} = \sigma_{ext} - \sigma_{sca} \qquad (5.20)$$

$$i_1 = \left| \sum_{n=1}^{\infty} \frac{2n + 1}{n(n+1)} |a_n(\alpha,m)\pi_n(\mu_s) + b_n(\alpha,m)\tau_n(\mu_s) \right|^2 \qquad (5.21)$$

$$i_2 = \left| \sum_{n=1}^{\infty} \frac{2n + 1}{n(n+1)} |a_n(\alpha,m)\tau_n(\mu_s) + b_n(\alpha,m) \ _n(\mu_s) \right|^2 \qquad (5.22)$$

where

$$\alpha = \frac{2\pi a}{\lambda}$$

a = d/2, radius of the particle

m = complex index of refraction = $n_1 - in_2$

$$\beta = m\alpha$$

$$a_n = \frac{\psi_n(\alpha)\psi_n'(\beta) - m\,\psi_n(\beta)\phi_n'(\alpha)}{\zeta_n(\alpha)\psi_n'(\beta) - m\,\psi_n(\beta)\zeta_n'(\alpha)}$$

$$b_n = \frac{\psi_n(\beta)\psi_n'(\alpha) - m\,\psi_n(\alpha)\psi_n'(\beta)}{\psi_n(\beta)\zeta_n'(\alpha) - m\,\zeta_n(\alpha)\psi_n'(\beta)}$$

$$\pi_n(\mu) = P_n'(\mu)$$

$$\tau_n(\mu) = \mu\rho_n(\mu) - (1-\mu^2)\pi_n'(\mu).$$

The P_n are Legendre polynomials and the ψ_n, ζ_n are Ricatti-Bessel functions. σ_{ext}, σ_{sca} and σ_{abs} are the extinction, scattering and absorption cross sections of the particle. i_1 and i_2 describe the patterns of scattered intensity polarized perpendicular and parallel to the scattering plane (determined by incident and scattered beams), respectively. For the unpolarized light treatment the pattern of scattered intensity is proportional to $i_1 + i_2$.

It can be shown that σ_{sca} is related to the integral of $i_1 + i_2$ over all scattering angles Ω_s:

$$\sigma_{sca}(\alpha) = \frac{1}{2}\left(\frac{\lambda}{2\pi}\right)^2 \int_{4\pi} [i_1(\alpha,\mu_s) + i_2(\alpha,\mu_s)]d\Omega_s \quad (5.23)$$

The numerical evaluation of the infinite series, Eqs. (5.18) through (5.22), while seemingly straightforward, has sources of error which are related to the accumulation of round-off error in recursively calculating ψ_n, ζ_n, π_n, and τ_n. Techniques to eliminate these errors have been discussed by numerous authors: Dave,[43] Kattawar and Plass,[44] and Denman, Heller, and Pangonis.[45]

The Mie equation reduces to two simple formulae for the limiting cases of large and small particles. If d is much less than λ, then we obtain Rayleigh scattering

$$\sigma_{sca}(\theta) = \frac{8}{\pi}\left(\frac{\pi d}{2\lambda}\right)^4\left(\frac{m^2-1}{m^2+2}\right)^2 (1 + \cos^2\theta). \quad (5.24)$$

The absorption cross section is given as

$$\sigma_{abs} = \frac{3\pi}{4\lambda} d^3 \, Im \frac{m^2-1}{m^2+2}. \quad (5.25)$$

If the particle is large compared to the radiation wavelength the wave character is relatively unimportant. Then the absorption cross section is

$$\sigma_{abs} = \frac{\pi d^2}{4} (1-\bar{R}), \qquad (5.26)$$

where $\bar{R}$ is the effective reflectance of the surface (averaged over incident angle).

Mie Scattering, Polydispersion

In reality, it is difficult to find particles of a single size. Rather, one is confronted with a situation in which there exist particles with a wide range of radii a. This variation is described by a size distribution function,

$$N\, n(a), \quad a_{min} \leq a \leq a_{max}$$

where N is the total number density of particles and n(a) is the normalized distribution of radii defined such that

$$n(a)\, da = \text{fraction of particles with radii at } (a,\ a + da)$$

$$\int_{a_{min}}^{a_{max}} n(a)\, da = 1$$

The volume scattering and absorption coefficients for polydispersions described by such a size distribution are:

$$\beta_\nu = N \int_{a_{min}}^{a_{max}} \sigma_{sca}(\alpha)\, n\,(a)\, da \qquad (5.27$$

$$\alpha_\nu = N \int_{a_{min}}^{a_{max}} \sigma_{abs}(\alpha)\, n(a)\, da. \qquad (5.28)$$

The pattern of scattered intensity will be proportional to

$$N \int_{a_{min}}^{a_{max}} [i_1(\alpha,\mu_s) + i_2(\alpha,\mu_s)]\, n(a)\, da.$$

Normalizing this so that its integral over all scattering directions Ω_s is 4π, we obtain the Mie phase function

$$\rho_\nu(\mu_s) = 4 \frac{\int_{a_{min}}^{a_{max}} [i_1(\alpha,\mu_s) + i_2(\alpha,\mu_s)]\, n(a)\, da}{\int_{4\pi} d\Omega_s \int_{a_{min}}^{a_{max}} [i_1(\alpha,\mu_s) + i_2(\alpha,\mu_s)]\, n(a)\, da}$$

Inverting the order of integration in the denominator and employing the relationships of Eqs. (5.23) and (5.27),

$$\rho_\nu(\mu_s) = \frac{\lambda^2 N}{\pi \beta_{\nu,M}} \int_{a_{min}}^{a_{max}} [i_1(\alpha,\mu_s) + i_2(\alpha,\mu_s)]\, n(a)\, da. \qquad (5.29)$$

Various analytic forms for n(a) can be assumed such as the Junge power-law distribution[46] $(ca^{-\gamma})$; Derimendjian's[47] modified gamma distribution $(ca^{\gamma}e^{-ba^{\delta}})$ or Log-normal distributions

$$\left(\frac{1}{\sigma\sqrt{2\pi}\, a} e^{-\ln^2(r/r_o)/2\sigma^2}\right).$$

Although the best size distribution is obtained from the experiments the calculations with different distributions can show the sensitivity of results leading to the accuracy with which the experimental values should be obtained.

5.4.3 Radiation Properties of Carbon Particles

Emission, absorption and scattering of radiation from carbon particles can be readily calculated once the ratio of particle size to wavelength of radiation, as well as the optical properties of the particles at that wavelength are known. These parameters when used in Mie scattering calculations yield the required quantities. To show the effect of wavelength and the size of the particle on the scattering and total cross sections, some results obtained by Stull and Plass[32] are presented in Fig. 5.4. Note that the scattering cross section decreases rapidly as the particle size decreases or the wavelength increases. Other important studies which discuss the radiation characteristics of or radiation from carbon particles are discussed in Refs. 33 and 34.

Emission and Scattering from Carbon Particle Size Distribution

As discussed before, the emission and scattering characteristics of particle size distribution can be calculated if these characteristics for each size are known. The calculations for evaluation of these cross sections are simplified considerably when the particle size is very small. Figures 5.5 and 5.6 show that the size distribution does have an important effect upon the cross sections and that for small size particles scattering is negligible.

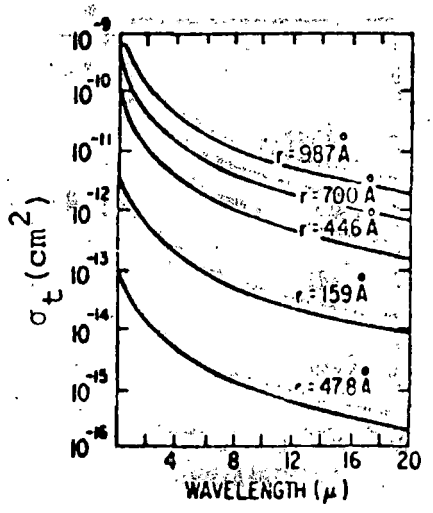

(a) total cross section, Q_t

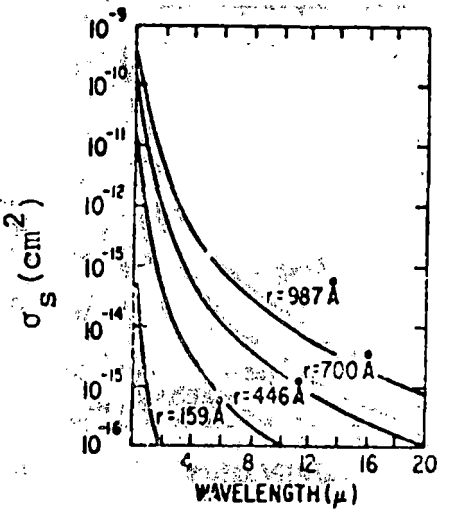

(b) scattering cross section, Q_s

Figure 5.4. Cross section as a function of wavelength for carbon particles of various radii.[32]

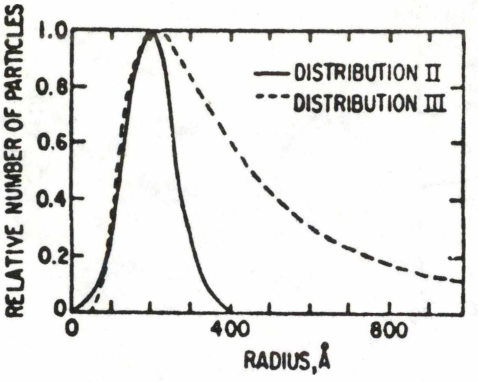

Figure 5.5. Two particle-size distribution used for the calculation of the emissivity of carbon particles.[ ] Distribution II: $N(r)dr = (N_p/159.52 \exp[-(r200)/90]^2\ dr$; distribution III: $N(r)dr = 4.75\ 10^5\ N_{pr}{}^{-3} \times [\exp(-640/r)]dr$ for $50 \leq r(Z) \leq 1000$ and $N(r)dr = 0$ for other values of r.

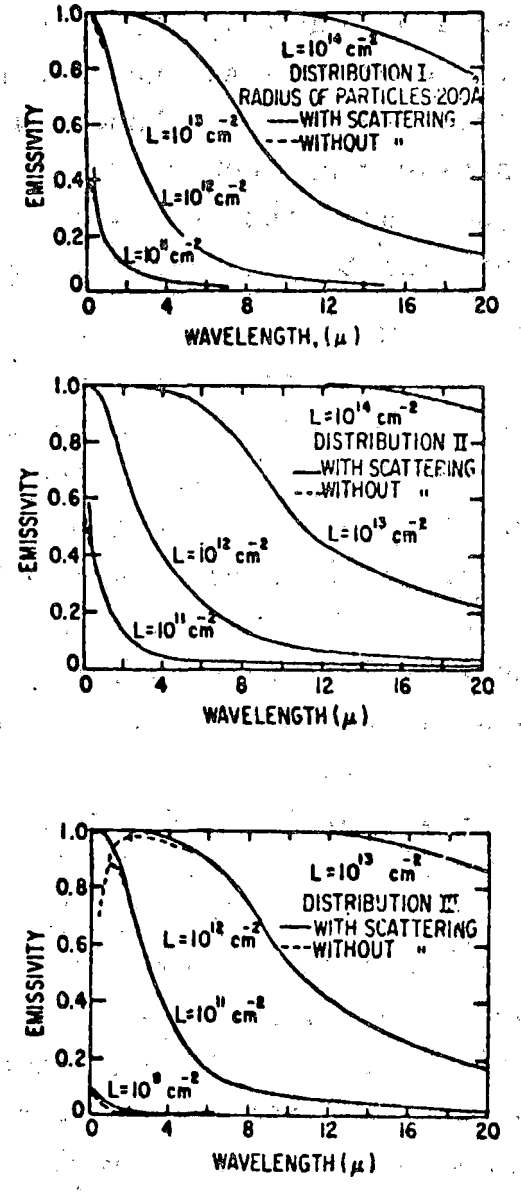

Figure 5.6. Emissivity as a function of wavelength for different particle-size distribution.[32]

5.5 STATUS OF THE RADIATION TRANSPORT CODE

During the initial quarter we have made operational a computer code, based on the long characteristics approach, which can calculate the net radiant heating rate at any location inside the fire. The code can handle axisymmetric fires with temperature, pressure and concentration gradients. Particulate matter such as carbon particles, as well as liquid droplets, can also be introduced into the fire.

At the present time the code contains the detailed radiation properties data of the main components of combustion, i.e., H_2O vapor, CO_2, CO and fine carbon powder over a wide wavelength and temperature range. The data for other constituents, especially fuels, has not been located so far in a useable form. The most detailed data of radiation properties of gaseous fuels, which we have been able to locate is published by American Petroleum Institute in their publication 44. The data is in the form of percent transmittance of a cell filled with the fuel gas, an example of which is shown in Fig. 5.3. This data for transmittance, must be reduced to absorption coefficient data before it can be used in the calculations. Also this data does not cover the spectrum below 2 μ which must be found from other sources. Since the three fuels, for which S^3 is to collect data, have not been chosen, it is difficult to concentrate on literature search. So far our main efforts have been directed at collecting radiation property data for propane gas.

The incorporation of liquid droplets, dust particles, appreciable size carbon particles into radiation calculations demands that absorption and scattering cross sections of single size particles as well as polydispersions be determined from Mie calculations. Mie scattering theory has been described above and is not simple. Although we have a code which can perform these calculations, it must be adapted to the particular needs of this problem. Moreover, the input property

data to the Mie scattering code, the real and complex parts of index of refraction as a function of wavelength for different materials, must be found and tabulated.

In the next quarter of this program our effort shall be directed to the above mentioned areas and to simplifying and streamlining the code. Major simplifications are expected, however, only after the code is run for real torch and pool fires.

VI. WORK FOR NEXT QUARTER

In the next quarter the torch fire code will be completed, the specified calculations made, and the code installed at the NASA-Ames computer center. In order to complete the code, the hydrodynamic part of the code and its associated chemical/equation of state package must be debugged, the droplet vaporization model added to the code and debugged, and the radiation subroutines "hooked on" to the resulting code. In order to perform the required calculations, the orifice diameter and two of the efflux rates of gaseous propane must be specified by NASA-Ames.

The pool fire code is, in many ways, similar to the torch fire code. The additional bouyancy terms that appear in the equations will be derived in the next quarter and incorporated into the pool fire version. We also expect to have completed our examination of the details of the initial (starting) conditions for the pool fire which are quite different from those of the torch. A search for material properties for the three fuels to be used in subsequent calculations will continue, but would be aided by a finalization of their specification.

Finally, detailed work including possibly some plume calculations for LNG spills will be initiated.

REFERENCES

1. Mikatarian, R. R., C. J. Kau, and H. S. Pergament, "A Fast Computer Program for Nonequilibrium Rocket Plume Predictions," Air Force Rocket Propulsion Laboratory Report AFRPL-TR-72-94, August 1972.

2. "A Proposal for Development of Analytic Fire Models," Systems, Science and Software Proposal P-74-1854, February 15, 1974.

3. Launder, B. E., and D. B. Spalding, "The Numerical Computations of Turbulent Flows," Imperial College of Science and Technology, Heat Transfer Section Report HTS/73/2, January 1973.

4. Spalding, D. B., B. E. Launder, and J. H. Whitelaw, "Turbulence Models and Their Experimental Verification," Notes for Lecture Series at Pennsylvania State University, April 8-10, 1974.

5. Lee, K. B., M. W. Thring, and J. M. Beer, "On the Rate of Combustion of Soot in a Laminar Soot Flame," Combustion and Flame, 6, pp. 137-145, 1962.

6. Thring, M. W., J. M. Beer, and P. J. Foster, "The Radiative Properties of Luminous Flames," Proceedings of the Third International Heat Transfer Conference, American Institute of Chemical Engineers, New York, 1966.

7. Radcliffe, S. W., and J. W. Appleton, "Shock Tube Measurements of Carbon to Oxygen Atom Ratios for Incipient Soot Formation with C_2H_2, C_2H_4, and C_2H_6 Fuels," Combustion Science and Technology, 3, pp. 255-262, 1971.

8. Ivernel, A., and G. Rousseau, "Formation of Carbon Black in Industrial Natural Gas Flames: Effect of Oxygen," Combustion Science and Technology, 5, pp. 193-194, 1972.

9. Maraval, L., "Characteristics of Soot Collected in Industrial Diffusion Flames," Combustion Science and Technology, 5, pp. 207-212, 1972.

10. Porter, G., Fourth Symposium (Int.) on Combustion, p. 248, William and Wilkins, Baltimore, 1953.

11. Hein, K., "Recent Results on the Formation and Combustion of Soot in Turbulent Fuel Oil and Gas Flames," Combustion Science and Technology, 5, pp. 195-206, 1972.

12. Tesner, P. A., and A. M. Tsibulevsky, "Gasification of Dispersed Carbon in Hydrocarbon Diffusion Flames," Combustion, Explosion and Shock Waves, 3, pp. 1963-1967, 1969.

13. Fenimore, C. P., and G. W. Jones, "Oxidation of Soot by Hydroxyl Radicals," J. P. Chem., 71, pp. 593-597, 1967.

14. Radcliffe, S. W., and J. W. Appleton, "Soot Oxidation Rates in Gas Turbine Engines," Combustion Science and Technology, 4, pp. 171-175, 1971.

15. Park, C., and J. P. Appleton, "Shock Tube Measurements of Soot Oxidation Rates," Combustion and Flame, 20, pp. 369-379, 1973.

16. Nagle, J., and R. F. Strickland-Constable, "Oxidation of Carbon Between 1000-2000°C," Proceedings Fifth Carbon Conference, 1, pp. 154-164, 1962.

17. Viskanta, R., "Radiation Transfer and Interaction of Convection with Radiation Transfer," in Advances in Heat Transfer (Edits. T. J. Irvine, Jr. and J. P. Hartnett), Vol. 3, Academic Press, New York, 1966.

18. Chandrasekhar, S., Radiative Transfer, Dover, New York, 1960.

19. Adrianov, V. N., Teploenerg, Vol. 8, No. 2, p. 63 1961.

20. Schuster, A., Astrophysics Journal, Vol. 21, p. 1 (1905).

21. Schwarzschild, K., Nachr. Akad. Wiss Goettingen, Math.-Physik. Kl. Vol. 1, p. 41 (1906).

22. Larkin, B. K., and S. W. Churchill, A.I. Ch.E. (Am. Inst. Chem. Engrs.) J., Vol. 5, p. 467, 1959.

23. Chen, J. C., A.I. Ch. E. (Am. Inst. Chem. Engrs.) J., Vol. 10, p. 253, 1964.

24. Milne, E. A., in Handbuch der Astrophysik (G. Eberhard, et al., Eds.), Vol. 3, Part 1, pp. 65-255, Springer, Berlin, 1930.

25. Eddington, A. S., The Internal Constitution of Stars, Dover, New York, 1959.

26. Kadanoff, L. P., J. Heat Transfer, Series C, Vol. 83, p. 215, 1961.

27. Goulard, R., "A Milne-Eddington Model in Heat and Mass Transfer," Report A. & E.S. 64-6, Purdue University, School of Aeronautical and Engineering Sciences, 1964.

28. Kourganoff, V., "Basic Methods in Heat Transfer Problems," Oxford University Press (Clarendon), New York, 1952.

29. Davison, B., "Neutron Transport Theory," Oxford University (Clarendon) New York, 1958.

30. Gosman, A. D., and F. C. Lockwood, "Incorporation of a Flux Model for Radiation into a Finite-Difference Procedure for Furnace Calculations," pp. 661-671, 14th.

31. Gosman, A. D., et al., Heat and Mass Transfer in Recirculating Flows, Academic Press, New York, 1969.

32. Toor, J. S., "Effect of Boundary Surface Characteristics on Reflectance of Solar Radiation from Shallow Bodies of Water," ASME Paper No. 73-WA/Sol-9.

33. Toor, J. S., and A. A. Boni, "Infrared Radiation Signatures from Turbine Powered Aircraft," Vol. 1, Phase II, Systems, Science and Software Report SSS-R-73-1707, 1973.

34. Penner, S. S., Quantitative Molecular Spectroscopy and Gas Emissivities, Addison-Wesley, 1959.

35. Penner, S. S., and D. B. Olfe, Radiation and Reentry, Academic Press, 1968.

36. Kondrat'Yev, K. Ya, Radiative Heat Exchange in the Atmosphere, Pergamon Press, 1965.

37. Goody, R. M., Atmospheric Radiation, 1. Theoretical Basis, Oxford Press, 1964.

38. Goody, R. M., "The Transmission of Radiation Through an Inhomogeneous Atmosphere," J. Atm. Sci., Vol. 21, 1964.

39. Walshaw, C. D., and C. D. Rogers, "The Effect of Curtis-Godson Approximation on the Accuracy of Radiative Heating-Rate Calculations," Quant. J. Roy. Met. Soc., 89, p. 422, 1963.

40. Zdunkowski, W. G., and W. H. Raymond, "Exact and Approximate Transmission Calculations for Homogeneous and Non-homogeneous Atmosphere," B. Zur Physik der Atmosp., Vol. 43, p. 185, 1970.

41. American Petroleum Association Publication, No. 44.

42. Van der Hulst, H. C., "Light Scattering by Small Particles," Wiley, New York, 1957.

43. Dave, J., "Effect of Varying Integration Increment on the Computed Polarization Characteristics of the Radiation Scattered by Polydispersed Aersols," Appl. Optics, 8, p. 2153, 1969.

44. Kattawar, G., and G. Plass, "Electromagnetic Scattering from Absorbing Spheres," Appl. Optics, 6, p. 1377, 1967.

45. Denman, H., W. Heller, and W. Pangonis, Angular Scattering Functions for Spheres, Wayne State University Press, Detroit, (D66).

46. Junge, C. E., Air Chemistry and Radioactivity, Academic Press, New York, 1963.

47. Deirmendjian, D., Electromagnetic Scattering on Spherical Polydispersions, Elsevier, New York, 1969.

48. Stull, V. R., and G. N. Plass, J. Opt. Soc. Am., 50, p. 121, 1960.

49. Boynton, F. P., et al., "Spectral Emissivity of Carbon Particle Clouds in Rocket Exhausts," AIAA J., 6, No. 5, 1968.

50. Simmons, F. S., "The Spectral Emissivity of Dispersed Carbon Particles in Rocket Exhaust Gases," Research Report 60-14, Rocketdyne.

Development of Analytical Fire Models,1974, US DOT, FRA, L Schalit, G Schneyer, J Toor, D Laird,14-HazMat